Mechanical Unfolding of Macromolecules Coupled to Bond Dissociation

Ariane Nunes-Alves and Guilherme Menegon Arantes*

Department of Biochemistry, Instituto de Química, Universidade de São Paulo, Av. Prof. Lineu Prestes 748, 05508-900 São Paulo, SP, Brazil

S *Supporting Information*

ABSTRACT: Single-molecule force spectroscopy has become a powerful tool to investigate molecular mechanisms in biophysics and materials science. In particular, the new field of polymer mechanochemistry has emerged to study how tension may induce chemical reactions in a macromolecule. A rich example is the mechanical unfolding of the metalloprotein rubredoxin coupled to dissociation of iron−sulfur bonds that has recently been studied in detail by atomic force microscopy. Here, we present a simple molecular model composed of a classical all-atom force field description, implicit solvation, and steered molecular dynamics simulation to describe the mechanical properties and mechanism of forced unfolding coupled to covalent bond dissociation of macromolecules. We apply this model and test it extensively to simulate forced rubredoxin unfolding, and we dissect the sensitivity of the calculated mechanical properties with model parameters. The model provides a detailed molecular explanation of experimental observables such as force−extension profiles and contour length increments. Changing the points of force application along the macromolecule results in different unfolding mechanisms, characterized by disruption of hydrogen bonds and secondary protein structure, and determines the degree of solvent access to the reactive center. We expect that this molecular model will be broadly applicable to simulate (bio)polymer mechanochemistry.
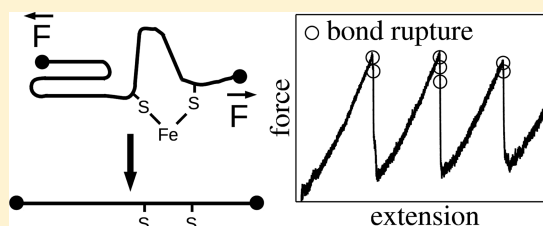
1. INTRODUCTION

The stability and denaturation kinetics of macromolecules are fundamental properties relevant to both natural polymers and designed materials. Besides the more traditional thermal and chemical unfolding techniques based on ensemble-averaged observations, polymer stability has been recently probed by mechanical manipulation at the single-molecule level, particularly by atomic force microscopy (AFM) and optical tweezer methods.[1−4]

These single-molecule force spectroscopy techniques are often applied to unfold polymers composed of repetitions of several folded units, leading to measured force−extension curves with a regular sawtooth pattern.[5] Increments in contour length between force peaks can be used as fingerprints to assign the specific macromolecular region unfolded under tension and attribute its stability to the distribution of measured peak forces.[6] Further information on the polymer unfolding kinetics can be obtained from experiments run at different pulling rates that depict the dependency of unfolding force on pulling velocity, also called the (dynamic) force spectrum of the material.[5,7−9]

Although studies have been performed most often in macromolecules that mechanically unfold only due to disruption of noncovalent interactions, there is an increasing number of studies reporting polymer mechanochemical activation: Si−O bond dissociation in stretched polydimethylsiloxane,[10] poly(tetrahydrofuran) detachment from a silver(I)−N−carbene complex,[11,12] iron−catechol complex dissocia-

tion,[13] and metal−amino acid bond rupture in different metalloproteins.[14−16] Another rich example is the mechanical unfolding of the metalloprotein rubredoxin coupled to the dissociation of ferric−thiolate (Fe−S) covalent bonds that has been extensively studied by AFM[17−22] and electronic structure calculations.[22−24]

Rubredoxin is a simple iron−sulfur protein with four cysteine side-chains S_γ bound to just one Fe atom in a tetrahedral orientation (Figure 1). This FeS center is buried in the polymer interior, and complete rubredoxin unfolding requires exposure to solvent and rupture of at least two of the four Fe−S bonds. Rubredoxin polyproteins, or polymerical constructions composed of repetitions of protein units, have been prepared by chemical cross-linking[25] or genetic engineering.[26] In the former case, protein units are connected through a pair of additional cysteine residues introduced in the rubredoxin sequence by point mutations. Polyproteins with different topologies have been prepared using this procedure, and their mechanical unfolding rate and force distributions were shown by AFM to depend on the points of force application along the rubredoxin sequence.[19]

Steered molecular dynamics (SMD) simulations[27,28] have been of great aid in the interpretation of mechanical unfolding experiments by providing a molecular picture and mechanistic details. For instance, SMD simulations revealed the molecular
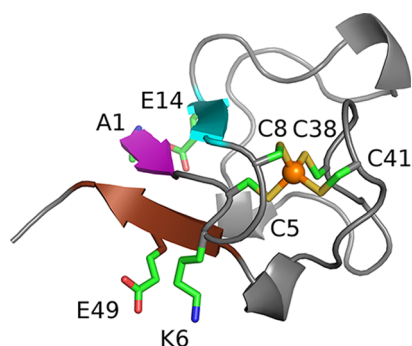
Figure 1. Rubredoxin crystal structure from *Pyrococcus furiosus*.[42] Fe is shown in orange; Cys bound to Fe and residues in salt bridges are shown as sticks. β-strands 1, 2, and 3 are indicated in pink, cyan, and brown, respectively.

basis for the plateau phase seen in fibrinogen force−extension curves[29] and that the mechanical stability of the titin I91 domain is due to contacts between β-strand pairs.[30,31]

Covalent mechanochemistry[32,33] and its effect on the stability of macromolecules[34,35] cannot be modeled with SMD employing classical force fields. These phenomena have traditionally been studied by quantum-chemical methods, where a small-molecule model system containing the disrupted bond is simulated by constrained geometry optimization[22,23,36−40] or by *ab initio* molecular dynamics.[33,40] Both approaches are computationally expensive and may not sample enough reactive events or orthogonal degrees of freedom. Such model and sampling limitations may hamper assignment of complete unfolding mechanisms and determination of rupture force spectra, distributions, and the influence of nonreactive but structurally important regions on the activated reaction center. Reactive force fields have recently been introduced as computationally efficient descriptions of reactive systems,[41] but, to our knowledge, this method has not yet been applied to simulate force spectroscopy.

Here, we introduce a simple molecular mechanical method to simulate forced unfolding of macromolecules coupled to covalent bond dissociation. The method may be used to depict the unfolding mechanism of a complete polymer with good sampling statistics of tens to hundreds of unfolding events. In the following Computational Methods section, we describe the energy model composed of an empirical all-atom force field for nonreactive atoms and a Morse potential to describe the reactive covalent bonds. In the Results section, the model is applied to simulate the forced unfolding of rubredoxin in several polyprotein constructions, and the data are compared to a collection of AFM experiments previously available on equivalent systems. We discuss the sensitivity of mechanical properties to model parameters and the different mechanisms

for complete unfolding obtained. We conclude that the presented method is appropriate to simulate force spectroscopy and mechanochemical activation of macromolecules in detail.

2. COMPUTATIONAL METHODS

2.1. Setup of Molecular Models. Two polymer models were used here: a single protein rubredoxin unit and a polyprotein with three units connected in line. These models are denoted $[A,B]_n$, where A and B indicate the position of a point mutation to Cys in each rubredoxin unit that allows for a polyprotein connection to form and $n = 1$ or 3 indicates the number of units in each model. The crystal structure of ferric rubredoxin from *Pyrococcus furiosus* (PDB code 1BRF[42]) was used for both models. Mutations were introduced manually using PyMOL.[43] In the polyprotein, rubredoxin units were connected in the N-to-C orientation by a 1,2-diethoxyethane linker bound to S_γ of the mutated Cys residues in each unit, as shown schematically in Figure 2. In AFM experiments, polyproteins are composed of 3−6 rubredoxin units connected by maleimide−thiol cross-linking chemistry that covalently attaches the mutated Cys residues in each unit by a linker molecule similar to 1,2-diethoxyethane but with an unknown (probably random) relative orientation.[17]

Forced unfolding of $[RD1,49]_{1,3}$ and $[RD15,49]_{1,3}$ models begins with predissociation of β-strands 1−3 (Figure 1), as suggested by the observation of prepeaks in experimental AFM force−extension profiles.[19] This was confirmed here by running exploratory pulling simulations (section 2.3) and observing the rupture of hydrogen bonds between β-strands 1−3. Models $[RD1,49]_{1,3}$ and $[RD15,49]_{1,3}$ used here for the remaining results were built from an initial configuration with this β-strand already dissociated. For the other polyproteins, a predissociation of the rubredoxin β-sheet was neither observed experimentally[19] nor modeled here.

2.2. Force Field and Simulation Details. Macromolecular interactions were described by the all-atom CHARMM27 empirical force field.[44,45] For the FeS center, covalent parameters for angles and dihedrals using the CHARMM functional form and Lennard−Jones parameters (ϵ_{Fe} = 0.048 kJ mol^{-1} and σ_{Fe} = 0.38 nm) were taken from previous work.[46] These covalent parameters are similar to other values proposed for rubredoxin.[47,48] Partial charges q_{Fe} = 1.04, q_{S_γ} = −0.45, and $q_{C\beta}$ = −0.18 for Cys were based on Mulliken population analysis of previous quantum chemical calculations on FeS mimetic compounds.[23,24] All unfolding simulations employed implicit solvation in the generalized Born surface area (GB/SA) form.[49] This was introduced to decrease the computational cost and allow extensive sampling of unfolding trajectories. The GB/SA approximation assumes instantaneous solvent reorganization, which may be invalid for very fast pulling, when the solvent distribution around the protein is not at equilibrium.
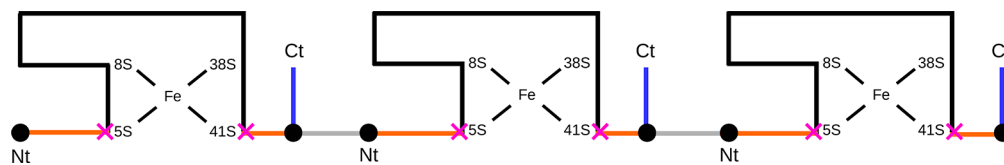

Figure 2. Schematic model of polyprotein $[RD1,49]_3$ used in the simulations. Rubredoxin units are connected by a linker (in gray). Black circles indicate the points of mutation (residues 1 and 49), pink crosses indicate the anchoring points (residues 5 and 41), orange lines indicate the regions under tension, blue lines indicate the regions outside the points of force application, black lines indicate the regions between anchoring points, and Nt and Ct indicate the protein termini. Positions of the Fe and native Cys S_γ centers are also indicated.

The Still method was used to estimate Born radii,[50] a dielectric constant $\varepsilon_r = 80$ was employed, and the nonpolar contribution was given by a uniform surface tension of 2.1 kJ mol^{-1} nm^{-2}.[51] The atomic radius for Fe was taken as 0.20 nm by comparison to other radii.

The four Fe−S bonds found in rubredoxin were represented by a Morse potential[52] to model bond dissociation during pulling simulations. Morse parameters were adjusted to quantum chemical calculations at the density functional level (DFT)[53] for the rate-limiting step of Fe−S bond dissociation in water for the Fe(SCH$_3$)$_4^-$ mimetic compound.[22] Steepness $\beta = 30$ nm^{-1} and depth $D_e = 90$ kJ mol^{-1} were adjusted so that the Morse potential reproduced the bond distance ($b^{\ddagger} = 0.34$ nm) and energy barrier ($\Delta E^{\ddagger} = 89$ kJ mol^{-1}) calculated with DFT for the mimetic transition state for the second Fe−S bond dissociation [Fe(SCH$_3$)$_3$OH$^-$ + H$_2$O; see Figure 5a of a previous publication[22]]. The equilibrium Fe−S bond distance set to $b_0 = 0.23$ nm was obtained from the isolated Fe(SCH$_3$)$_4^-$ optimized geometry.

Initial single rubredoxin and polyprotein models were submitted to geometry optimization and molecular dynamics (MD) simulation during ∼200 ns with position restraints (50 kJ mol^{-1} nm^{-2}) applied to the first N-terminal and the last C-terminal mutated Cys residue. Configurations used to start the pulling simulations were collected at regular time intervals (4−10 ns) after stabilization of the Cα root mean-squared deviation (RMSD).

Potential energy curves for Fe−S bond dissociation in the rubredoxin model were obtained by geometry optimization with the BFGS algorithm.[54,55] The Fe−S bond was scanned by restraining the Fe−S distance of Cys41 by a harmonic potential with force constant $k = 10^5$ kJ mol^{-1} nm^{-2}.

GROMACS 4.5[56] was used for all simulations and for building hydrogen atoms on the protein models. Dynamics were carried out at 300 K with a 2 fs time step, with a leapfrog stochastic dynamics integrator and a collision frequency $\tau = 10$ ps^{-1}. Covalent bonds between hydrogens and heavy atoms were constrained with LINCS.[57]

2.3. Forced Unfolding Simulations.
Forced unfolding trajectories were obtained using SMD simulations.[27] A time-dependent harmonic potential ($V[\xi]$) was added to the system energy function to mimic protein pulling by the cantilever or pulling tip on force spectroscopy experiments

$$V[\xi(t)] = \frac{k_p}{2}[\xi(t) - \xi_0(t)]^2 \tag{1}$$

where the reference value of the progress coordinate, ξ_0, changes linearly in time

$$\xi_0(t) = \xi(0) + v_p t \tag{2}$$

Simulations with constant velocity were performed with $v_p = 10^{-1}$ m s^{-1} and pulling force constant $k_p = 83$ pN nm^{-1}. Structures and forces were saved every 5 ps for analysis.

The progress coordinate ξ was defined as the distance between Cα in a reference center and in a pulling center. When pulling by the C-terminal, the reference center was set to the first N-terminal mutated Cys residue and the pulling center was set to the last C-terminal mutated Cys. For example, in model [RD15,49]$_3$ the reference center was C15 in the first rubredoxin unit and the pulling center was C49 in the third rubredoxin unit. Reference and pulling centers were exchanged when pulling by the N-terminal.

SMD simulations were initialized with a different random seed for stochastic dynamics and a different initial structure (section 2.2). Between 35 and 40 unfolding simulations were obtained for each polyprotein model, resulting in $N = 105-120$ complete unfolding events. Complete unfolding of models [RD1,49]$_1$ and [RD1,49]$_3$ takes ∼150 and ∼450 ns, respectively, with a velocity $v_p = 10^{-1}$ m s^{-1}. A Fe−S bond with a distance longer than 0.37 nm was considered broken. After each bond rupture, the simulation was paused and the associated angle and dihedral contributions were removed from the system topology. The trajectory was then continued from the same geometry.

Secondary structural content along trajectories was analyzed by counting the involved hydrogen bonds. The sheets between β-strands 1−2 and 1−3 (Figure 1) were considered formed when at least two of the hydrogen bonds found in the crystal structure were present.

2.4. Calculation of Contour Lengths.
Contour length (Lc) may be defined as the polymer extension at infinite force.[58] In AFM experiments of polyprotein unfolding, contour length increments (ΔLc^{AFM}) are obtained by fitting peaks in force−extension profiles to the worm like chain (WLC) model[59] and taking the difference between fitted Lc values from consecutive peaks.

Here, length increments were estimated as ΔLc = Lc(u) − Lc(f), where Lc is the distance between anchoring points before (f) and after (u) protein unfolding. Lengths will be labeled by a superscript indicating values obtained from sequences and crystal structures (PDB), SMD simulations, or AFM experiments. Anchoring points are the points of force application along the polymer. For proteins, they are defined as the amino acids enclosing the region unfolded in the corresponding peak in force−extension profiles[19] (see Table 2 for models studied here).

Lc(f)^{SMD} was obtained from the through-space distance between the Cα of anchoring points one frame before the first Fe−S bond rupture, preceding protein unfolding indicated by the respective force peak in the force−extension profiles. Lc(u)^{SMD} was taken as the distance between the same Cα's in the frame before the next force peak is achieved. Thus, the length increment estimated from SMD simulations (ΔLc^{SMD}) is slightly smaller as it corresponds to a polymer extension released at finite force. However, the difference to the true contour length should be small as it goes to zero with the inverse square root of the pulling force[59] and high forces (hundreds of pN) are applied in the SMD simulations here. We check this approximation to be valid by comparing ΔLc^{SMD} estimated as described with fitting the same simulation data to the WLC model (section 3.2).

As in previous works,[17,19] Lc(f)^{PDB} was calculated as the through-space distance between the Cα of anchoring points in the crystal structure. Lc(u)^{PDB} was estimated as $(n - 1) \times 0.365$ nm, where n is the number of amino acids between anchoring points and 0.365 nm is the average contribution in length per amino acid.[17,19,60]

3. RESULTS

3.1. Analysis of Simulation Parameters.
A sensitivity analysis of calculated mechanical properties due to variations in simulation parameters is presented in this section for the rubredoxin model [RD1,49]$_1$, except when noted. Only one type of parameter was varied for each set of simulations shown

Table 1. Average Rupture Forces ($\overline{F}$, Average ± Standard Deviation in pN) Calculated for the First Fe–S Bond Rupture in $[RD1,49]_1$ ($N = 10$ Simulations) with Different Values of Depth (D_e, kJ mol^{-1}) and Steepness (β, nm^{-1}) of the Morse Potential and Partial Charges q_{Fe} and q_S Assigned to the FeS Center[a]

D_e	$\overline{F}$	β	$\overline{F}$	q_{Fe}	q_S	$\overline{F}$
70	415 ± 78	15	348 ± 60	1.44	−0.55	525 ± 42
90	758 ± 127	20	530 ± 35	1.04	−0.45	758 ± 127
130	1632 ± 57	30	758 ± 127	0.64	−0.35	995 ± 75
170	2437 ± 118	40	1007 ± 88	0.24	−0.25	1163 ± 65

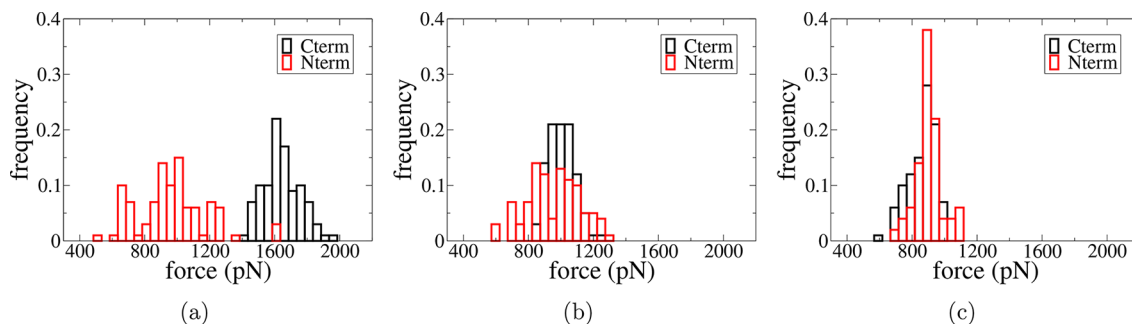[a]Only one type of parameter was changed in each set of simulations.

Figure 3. Distribution of rupture forces obtained for $N = 70-100$ simulations with pulling velocities $v_p = 10$ m s^{-1} (a), $v_p = 1$ m/s (b), and $v_p = 10^{-1}$ m s^{-1} (c) of model $[RD1,49]_1$.
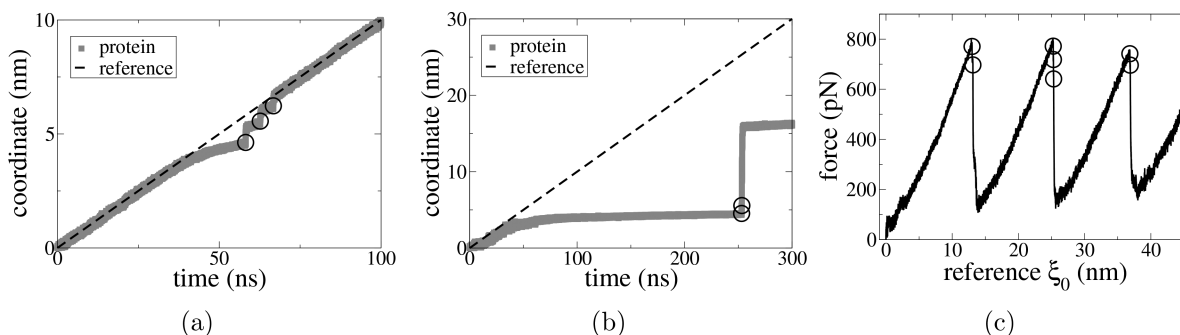

Figure 4. Time evolution of the reference progress coordinate (ξ_0, eq 2) and the protein extension coordinate for model $[RD1,49]_1$ obtained with a pulling force constant $k_p = 1667$ pN nm^{-1} (a) and $k_p = 83$ pN nm^{-1} (b). One representative force–extension curve simulated with $k_p = 83$ pN nm^{-1} for model $[RD1,49]_3$ is shown in panel c. Circles indicate Fe–S bond rupture.

below, while the others remained with values given in the Computational Methods section.

Table 1 shows that average rupture forces strongly depend on the Morse potential depth and steepness and on partial charges for FeS atoms, particularly when more polarized charges are used. Average forces are clearly more sensitive to changes in the Morse depth. Increasing the depth by 1.5-fold increases the forces by almost 6-fold. More polarized charges lead to lower rupture forces, probably due to stabilization by the dielectric solvent when the FeS center is exposed.

Potential energy profiles for Fe–S bond rupture are affected by the same force field parameters (D_e, β, and $q_{Fe/S}$ in Figure S1). This is expected given the derivative relation between dissociation energies and forces. The Morse steepness determines both the profile inclination and the Fe–S distance for bond dissociation.

On the other hand, Lennard–Jones σ_{Fe} and ϵ_{Fe} parameters and the atomic radius for Fe used in GB calculations have a small influence on potential energy curves for Fe–S bond dissociation (Figure S2), except when a low GB radius and σ were tested, which led to premature Fe–S dissociation before force application. Values for these parameters were chosen

based on previous calibrations[23,46] to avoid strong interactions between Fe and side chains with negative charge, and an unbalanced solvation contribution.

Figure 3 shows that the pulling velocity (v_p, eq 2) dramatically changes the distribution of rupture forces for the Fe–S bond. For very high velocities ($v_p = 10$ m s^{-1}), the distribution depends on the pulling direction. Decreasing the velocity removes this dependency, but only velocities down to $v_p \leq 0.1$ m s^{-1} result in a force distribution with the expected bell shape[28,61] and a standard deviation compatible with the experimental one ($\sim$150 pN).[17]

Average rupture forces obtained with a pulling velocity of $v_p = 0.1$ m s^{-1} are similar between model $[RD1,49]_1$ ($\overline{F} = 758 \pm 127$ pN, $N = 11$ unfolding events) and model $[RD1,49]_3$ pulled either by the C-terminal ($\overline{F} = 738 \pm 93$ pN, $N = 69$) or by the N-terminal ($\overline{F} = 744 \pm 86$ pN, $N = 33$). Mechanistic details and the sequence of structural changes for complete unfolding (section 3.3) are also equivalent between models $[RD1,49]_1$ and $[RD1,49]_3$.

The pulling force constant (k_p) does not significantly affect the rupture force (Table S1), but it controls the shape of the force–extension curves (Figure S3). High force constants result

in distinct peaks for each Fe−S bond rupture and hence result in multiple peaks for a complete protein unfolding event. One peak followed by a continuos relaxation curve, as observed experimentally,[17,19] is obtained from simulation only when decreasing the force constant to about twice the experimental value (40 pN nm^{-1}).[17]

Figure 4 shows that the protein extension measured from termini Cα distances follows the harmonic pulling potential or reference coordinate (ξ_0, eq 2) only when a high pulling force constant is used. When a low force constant similar to the experimental value is used, the protein extension does not strictly follow the reference pulling coordinate. Figure 4 also shows that the maximum force in force−extension profiles is reached just before the first Fe−S bond rupture.

Slower pulling velocities and lower force constants considerably increase the amount of computer time necessary for simulating protein unfolding. For instance, complete unfolding of the $[RD1,49]_1$ model with a pulling velocity v_p = 10^{-2} m s^{-1} takes about 3 weeks of wall-clock time on modern Intel Xeon processors using 4 CPU cores, which is the highest number of cores that a decent parallel scalability was observed for such a molecular model with a relatively small number of particles.

3.2. Comparison between SMD and AFM Data. A comparison between unfolding forces observed in SMD simulations and AFM experiments is not straightforward as simulations have to be conducted at much higher pulling velocities than AFM, except in (rare) experiments when high speeds are realized.[7,62] For rubredoxin unfolding, there is a gap of almost 4 orders of magnitude between our slowest pulling simulation and the fastest measurement,[19] as shown for the force spectrum in Figure 5.
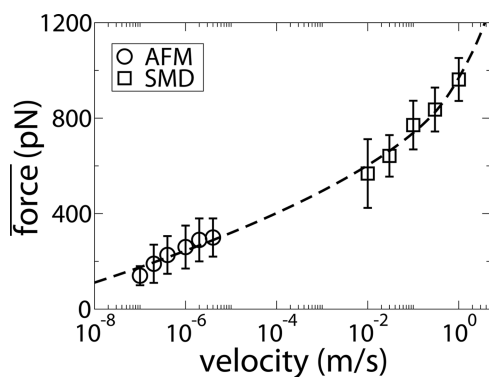

Figure 5. Force spectra or average rupture forces obtained at different pulling velocities for AFM experiments[19] and SMD simulations (N = 20) of model $[RD1,49]_1$. The dashed line shows the full microscopic model derived by Hummer and Szabo[61] fitted to both AFM and SMD data. Error bars in SMD points indicate one standard deviation.

However, the dependency of unfolding forces on pulling velocities has been studied by theory in detail.[28,61,63−66] In Figure 5, we also show adjustment of the full microscopic theoretical model derived by Hummer and Szabo[61] to fit SMD and AFM force spectra for rubredoxin unfolding. The fit quality is rather good with a mean deviation of 22 pN between the model line and data points. The theoretical model predicts an unfolding barrier position $\Delta x^{\ddagger}$ = 0.17 nm and a spontaneous unfolding rate k_0 = 0.22 s^{-1}, in good agreement with the barrier position and spontaneous rate obtained by fitting the AFM data alone either with the same theoretical model ($\Delta x^{\ddagger}$ = 0.11 nm

and k_0 = 1.0 s^{-1}) or with a simplified phenomenological theory[64] ($\Delta x^{\ddagger}$ = 0.11 nm and k_0 = 0.15 s^{-1}).[19]

Additionally, by assuming the microscopic theoretical model[61] is valid, the force field parameters (for instance, Morse β and D_e as shown in Figure S4) can be refined by comparison of the experimental AFM force spectra with SMD simulations obtained with different sets of parameters.

Comparison between simulated and AFM contour length increments in Table 2 shows excellent agreement for polyproteins $[RD15,49]$ and $[RD15,35]$ and good agreement for polyprotein $[RD1,49]$, considering one standard deviation and the two experimental results available.[17,19] Simulated and AFM increments only disagree for $[RD1,35]$.

It should be noted that the procedure based on WLC fits to obtain ΔLc from AFM data and that based on Cα distances described in section 2.4 give equivalent results when applied to the same set of simulated force−extension profiles. For example, the same set of N = 8 simulated unfolding events for model $[RD1,49]_3$ resulted in ΔLc^{SMD} = 12.2 $\pm$ 0.5 nm when using Cα distances and ΔLc^{SMD} = 12.5 $\pm$ 0.7 nm when using WLC fits. Equivalent results are observed for other rubredoxin polyproteins.

Table 2 shows that length increments expected from crystal structures (ΔLc^{PDB}) are overestimated in comparison with the increments obtained from simulations (ΔLc^{SMD}) for all polyprotein models, except $[RD1,49]_3$. Closer inspection indicates that $Lc(u)^{PDB}$ and $Lc(u)^{SMD}$ are in very good agreement. Thus, discrepancies in ΔLc increments are due to underestimated $Lc(f)^{PDB}$ values, based on the unperturbed crystal structure.

3.3. Microscopic Mechanism for Forced Macromolecular Unfolding. Pulling simulations of polyprotein models were also used to describe the detailed mechanism of rubredoxin mechanical unfolding. In the beginning of all simulations, linker and protein regions connecting rubredoxin units were first extended without much perturbation in the rest of the molecular structure (time t < 50 ns in Figure 4b). Then, tension starts to build up and little extension is gained until the Fe−S bonds are broken (50 < t < 250 ns in Figure 4b). During this second phase, structural fluctuations are relatively small in the regions under tension and between anchoring points (see these regions depicted in Figure 2).

Table 3 shows the stability of secondary structures and salt bridges found in rubredoxin along pulling simulations. Contacts between β-strands 1−2 are preserved before Fe−S bond rupture in all $[RD1,49]_3$ and $[RD1,35]_3$ simulations, but they are disrupted in all $[RD15,49]_3$ and $[RD15,35]_3$ simulations. Hydrogen bonds between β-strands 1−3 are preserved before Fe−S bond rupture in half of the simulations for $[RD15,35]_3$ and for the majority of $[RD1,35]_3$ simulations. The stability of salt bridges A1−E14 and K6−E49 follows the same qualitative pattern, although they are less stable. Notice that the wild-type salt bridge between residues 6 and 49 is not present in $[RD1,49]_3$ and $[RD15,49]_3$ due to the E49C mutation.

Exploratory pulling simulations showed that contacts between β-strands 1−3 are disrupted early for models $[RD1,49]_3$ and $[RD15,49]_3$ during the first extension phase described above. Low force peaks corresponding to dissociation of hydrogen bonds between β-strands 1−3 are observed in the simulated force−extension profiles only for these models ($[RD1,49]_3$ and $[RD15,49]_3$, data not shown), in agreement with experimental AFM data.[19]

Table 2. Contour Lengths (Lc, Average ± Standard Deviation in nm) before (f) and after (u) Polyprotein Unfolding and Increments (ΔLc) Obtained from the Crystal Structure (Lc^{PDB}), AFM Experiments (Lc^{AFM}),[19] and SMD Simulations (Lc^{SMD}, N = 70−80 Values)^a

model	ΔLc^{PDB}	ΔLc^{SMD}	ΔLc^{AFM}	
[RD1,49]$_3$	12.2	12.0 ± 0.1	13.0 ± 0.8[19] and 12.6 ± 1.3[17]	
[RD15,49]$_3$	7.4	6.0 ± 0.1	6.4 ± 0.7	
[RD15,35]$_3$	5.3	2.7 ± 0.1	2.7 ± 0.4	
[RD1,35]$_3$	10.4	9.0 ± 0.1	11.1 ± 1.2	
	Lc(f)^{PDB}	Lc(f)^{SMD}	Lc(u)^{PDB}	Lc(u)^{SMD}	anchoring points
[RD1,49]$_3$	0.9	1.0 ± 0.1	13.1	13.0 ± 0.1	5, 41
[RD15,49]$_3$	2.1	3.3 ± 0.1	9.5	9.3 ± 0.1	15, 41
[RD15,35]$_3$	2.0	4.5 ± 0.1	7.3	7.2 ± 0.1	15, 35
[RD1,35]$_3$	2.0	3.3 ± 0.1	12.4	12.3 ± 0.1	1, 35

^{a}Residue number of anchoring points is also indicated.

Table 3. Fraction of Proteins with Salt Bridges and Secondary Structure Preserved before the First Fe−S Bond Rupture along Pulling Simulations (N = 105−120 Unfolding Events)^a

model	salt bridges		β-sheet	
	A1−E14^b	K6−E49	strands 1−2	strands 1−3
[RD1,49]$_3$	0.34	−	1.00	−
[RD15,49]$_3$	0.00	−	0.00	−
[RD15,35]$_3$	0.00	0.37	0.00	0.52
[RD1,35]$_3$	0.38	0.67	1.00	0.81

^{a}Residue and β-sheet numbering and positions are shown in Figure 1. Salt bridge K6−E49 and the contact between β-strands 1−3 were absent by construction in models [RD1,49]$_3$ and [RD15,49]$_3$. ^{b}C1−E14 in [RD1,49]$_3$ and [RD1,35]$_3$.

Cooperativity in the stability of salt bridges and secondary structures before Fe−S bond rupture also depends on the polyprotein connectivity. For instance, in model [RD15,35]$_3$ the survival of interactions overlap for the salt bridge A1−E14 and the hydrogen bonds holding together β-strands 1−2, meaning that these contacts are disrupted simultaneously (Figure S6). However, in model [RD15,49]$_3$, the salt bridge is disrupted first, followed sequentially by disruption of hydrogen bonds in β-strands 1−2. When salt bridges and secondary structures are disrupted before Fe−S bond dissociation, disruption is observed at the first half of the simulation time necessary to break the Fe−S bond (Figure S6).

Hydrogen bonds are found in the rubredoxin crystal structure (Figure 1) between S$_\gamma$ in the FeS center and backbone amides. S$_\gamma$Cys41 makes one hydrogen bond that is broken before Fe−S bond rupture during all pulling simulations for models [RD1,49]$_3$ and [RD15,49]$_3$. Tension is applied to the Fe−S$_\gamma$Cys41 bond on these models. S$_\gamma$Cys8 also makes one hydrogen bond, and it is equivalently disrupted in [RD15,35]$_3$ and [RD15,49]$_3$. On the other hand, S$_\gamma$Cys5 and S$_\gamma$Cys38 make two hydrogen bonds each, and these two are preserved before Fe−S bond rupture in all pulling simulations, except for 20% of the [RD1,35]$_3$ trajectories. Consequently, solvent access is considerably higher near S$_\gamma$Cys41 in [RD1,49]$_3$ and [RD15,49]$_3$ and near S$_\gamma$Cys8 in [RD15,35]$_3$ and [RD15,49]$_3$. For polyprotein [RD1,35]$_3$, solvent access is similar for both S$_\gamma$Cys5 and S$_\gamma$Cys38.

4. DISCUSSION

We have presented a molecular model to study the mechanical unfolding of a macromolecule coupled to covalent bond rupture and shown its application to simulate the forced unfolding of the rubredoxin metalloprotein.

A sensitivity analysis of calculated properties shows that parameters for the reactive center describing partial atomic charges and the Morse potential for bond dissociation have to be carefully calibrated as they have a large influence on rupture forces (Table 1 and Figure S1). Here, these parameters were adjusted to quantum chemical calculations at the DFT level performed on an isolated mimetic molecule and further refined in comparison to experimental data. In particular, the force spectra can be used to distinguish which parameter set better fits a microscopic theoretical model in comparison to AFM data (Figure S4). Less sensitive parameters such as those describing Lennard-Jones interactions can be retrieved from force fields previously parametrized for equilibrium properties.

This model for bond dissociation and the proposed approach for calibration are viable only if the chemical bonds disrupted upon mechanical unfolding are previously known or at least suggested. If two or more bonds can dissociate, each of them would have to be calibrated to a characteristic set of Morse parameters, as is often done in reactive force fields.[41] Here, the four Fe−S bonds found in rubredoxin were proposed to dissociate and treated with the same Morse potential. Of course it is expected that the force field description for the remaining nonreactive atoms in the macromolecule can properly model their interactions.[44,45]

The major limitation of our energy model is the classical description of the disrupted bond. The lack of an electronic structure or quantum chemical description prevents the inclusion of charge and spin reorganization effects in the simulation. These effects are important to model reactions involving organic and metal centers[23] and to discern details of reaction mechanisms and of the directionality of metal−ligand interactions. Thus, we are unable to use the rubredoxin simulations shown here to distinguish the order that each of the four possible Fe−S bonds is broken to complete protein unfolding.

The effect of the pulling force constant (k_p) on the simulated force−extension curves can be rationalized. When a high constant is used, protein extension strictly follows the harmonic pulling reference coordinate (Figure 4a) and samples only local forces, similar to the drift regime proposed before.[28] Complete unfolding is observed after multiple bond rupture steps, leading to multiple force peaks in force−extension curves. When a low force constant is used, the protein extension can fluctuate more and does not strictly follow the harmonic pulling coordinate (Figure 4b), similar to an activated regime.[28] The reaction

coordinate may also sample thermal forces, and more tension may accumulate. Complete unfolding is observed in one step, leading to one force peak in the force−extension curves, which corresponds to the first Fe−S bond rupture, quickly followed by disruption of other Fe−S bonds.

The force spectrum obtained from SMD and AFM data on rubredoxin unfolding was well adjusted here by the full microscopic model proposed by Hummer and Szabo[61] that assumes the rupture energy is described by a cusp potential. Although similar theoretical models based on smooth potentials have also been proposed,[66] their adjustment to force spectra obtained at high speeds did not lead to significant changes on the derived barrier position and unfolding rate.[7] This suggests some independence of adjusted parameters on the exact form of the rupture potential. Thus, the microscopic model[61] can be employed to fit the force spectrum when unfolding is coupled to covalent bond dissociation as modeled here by a smooth Morse potential.

Simulated and experimental contour length increments are in very good agreement for three of the four polyproteins studied here. Lengths before unfolding [Lc(f)] have traditionally been estimated from through-space distances between anchoring points on the macromolecular crystal structure. This may not be a reliable practice, as our comparison of Lc(f)^{PDB} and Lc(f)^{SMD} suggests. The coupling of protein units and force application before bond rupture perturb the structure of each unit and hence the distance between anchoring points (Table 2).[67] On the other hand, construction and simulation of polyprotein models require more labor than inspecting the crystal structures.

Notice the excellent agreement between lengths after unfolding Lc(u) obtained from SMD simulations and estimated from the formula $(n − 1) \times 0.365$ nm, where n is the number of amino acids between anchoring points (Table 2). Here, $(n − 1)$ is used in the formula instead of n adopted before[17,19] because the combined extension of the two residues in anchoring points will contribute only one length unit to Lc(u). Other values of contour length per amino acid proposed in the literature (0.38 and 0.40 nm)[58,67] result in disagreement between Lc(u)^{PDB} and Lc(u)^{SMD}, either using n or $(n − 1)$ as the number of amino acids.

Cavagnero et al.[68] proposed a mechanism for thermal denaturation of rubredoxin in three steps: rubredoxin first loses part of the secondary structure; Fe−S bonds are broken, iron is released, and more secondary structure is lost; and the hydrophobic core is exposed, leading to the unfolded state. This is based on data obtained by several optical spectroscopy methods at low pH, when Glu14 and Glu49 side chains should be protonated and their respective salt bridges should be broken.[69] Nevertheless, this proposed mechanism is roughly the sequence we obtain from mechanical unfolding simulations in polyproteins [RD15,35]$_3$ and [RD1,49]$_3$. Solvent exposure of the hydrophobic core varies for each polyprotein model, but it is also correlated with disruption of secondary structure.

The mechanism of macromolecular unfolding simulated here clearly depends on the points of force application along the polymer. Salt bridges and hydrogen bonds holding secondary structures together may be completely disrupted before covalent bond dissociation, as seen in rubredoxin model [RD15,49]$_3$, or almost entirely preserved, as seen in model [RD1,35]$_3$. The fraction of these intramolecular contacts present before Fe−S bond rupture in the four polyprotein models tested here increases in the order [RD15,49]$_3$ <

[RD15,35]$_3$ < [RD1,49]$_3$ < [RD1,35]$_3$. This is approximately the same order found for the average rupture force and the reverse order found for the intrinsic rate of unfolding k_0 on AFM measurements,[19] suggesting that the stability of intramolecular noncovalent contacts plays a role on macromolecules subject to mechanochemical activation.

Solvent exposure of the macromolecular interior and water access to the reactive FeS center in rubredoxin are controlled by partial protein unfolding, with disruption of secondary structures and of native hydrogen bonds between S$_\gamma$ and backbone amides. Our simulations show that water penetration is higher near S$_\gamma$Cys41 and S$_\gamma$Cys8, suggesting the respective Fe−S bonds would be more reactive than the other two. In fact, it has been shown by quantum-chemical calculations that water substitution leads to faster Fe−S bond cleavage in rubredoxin models.[22]

Thus, the mechanical anisotropy previously observed in rubredoxin polyproteins[19] may not be only due to differences in the intrinsic stabilities among the four Fe−SCys bonds[17,19] but also because of the variable degree of solvent access to the FeS center found here between different polyproteins.

Two types of mechanism for Fe−S bond rupture in mechanical unfolding of rubredoxin have been observed for a structural variant of rubredoxin.[20] A concurrent process, where multiple Fe−S bonds rupture simultaneously, was observed in 80% of AFM force−extension profiles, and a sequential mechanism, where rupture of different Fe−S bonds can be individually distinguished, was observed in the other 20% of AFM profiles. Observation of simultaneous processes depends on the time resolution of measurements, which is on the order of microseconds or slower for the mentioned AFM experiments. In our simulations, bond ruptures in the same protein unit are separated by tens of picoseconds. Therefore, within a microsecond time window, bond rupture occurs simultaneously in all simulations. It is possible that the sequential process observed in the AFM experiments is due to the protein construction containing an extra unnatural loop elongation in the studied rubredoxin variant.[20]

We conclude that the molecular mechanical model presented here may be applied to study the forced unfolding of macromolecules coupled to covalent bond rupture. Empirical force field parameters for bond dissociation can be obtained from quantum-chemical calculations on model compounds and further refined in comparison to experimental force spectra. SMD simulations revealed the mechanism of macromolecular unfolding and the sequence that intramolecular contacts are disrupted for four different polyproteins. Solvent penetration near the reactive center may be determinant for the mechanical stability of each polymer.

The simulation methods presented here are not limited to proteins. They can be applied to simulate forced unfolding and mechanochemical activation of any macromolecule for which an appropriate model of the molecular structure and a set of cleavable covalent bonds are known.

Given the lack of an electronic structure description of the reactive center in our classical model, the detailed mechanism and sequence of Fe−S bond rupture in the stretched rubredoxin models could not be analyzed. These would require a hybrid quantum chemical/molecular mechanical energy model, which we have been investigating in our laboratory.[23] Nevertheless, unfolding trajectories extensively sampled here with a computationally cheap method may be of great value as initial reactive conformations in future studies.

ASSOCIATED CONTENT

⑤ Supporting Information

The Supporting Information is available free of charge on the ACS Publications website at DOI: 10.1021/acs.jctc.7b00805.

> Potential energy profiles for Fe−S bond dissociation with different force field parameters, force spectra obtained with different Fe−S Morse potentials, time evolution of protein interactions, force−extension curves, scheme of rubredoxin mutants, and a table with average rupture forces with different pulling force constants (PDF)

AUTHOR INFORMATION

Corresponding Author

*E-mail: garantes@iq.usp.br.

ORCID ⊙

Guilherme Menegon Arantes: 0000-0001-5356-7703

Notes

The authors declare no competing financial interest.

REFERENCES

(1) Fisher, T. E.; Oberhauser, A. F.; Carrion-Vazquez, M.; Marszalek, P. E.; Fernandez, J. M. The study of protein mechanics with the atomic force microscope. *Trends Biochem. Sci.* **1999**, *24*, 379−384.

(2) Neuman, K. C.; Nagy, A. Single-molecule force spectroscopy: optical tweezers, magnetic tweezers and atomic force microscopy. *Nat. Methods* **2008**, *5*, 491−505.

(3) Passeri, D.; Rossi, M.; Tamburri, E.; Terranova, M. L. Mechanical characterization of polymeric thin films by atomic force microscopy based techniques. *Anal. Bioanal. Chem.* **2013**, *405*, 1463−1478.

(4) Kilpatrick, J. I.; Revenko, I.; Rodriguez, B. J. Nanomechanics of cells and biomaterials studied by atomic force microscopy. *Adv. Healthcare Mater.* **2015**, *4*, 2456−2474.

(5) Schönfelder, J.; De Sancho, D.; Perez-Jimenez, R. The power of force: insights into the protein folding process using single-molecule force spectroscopy. *J. Mol. Biol.* **2016**, *428*, 4245−4257.

(6) Franco, I.; Ratner, M. A.; Schatz, G. C. In *Nano and Cell Mechanics: Fundamentals and Frontiers*; Espinosa, H. D., Bao, G., Eds.; John Wiley & Sons: Chichester, UK, 2013; Chapter 14, pp 359−388.

(7) Rico, F.; Gonzalez, L.; Casuso, I.; Puig-Vidal, M.; Scheuring, S. High-speed force spectroscopy unfolds titin at the velocity of molecular dynamics simulations. *Science* **2013**, *342*, 741−743.

(8) Ando, T.; Uchihashi, T.; Scheuring, S. Filming biomolecular processes by high-speed atomic force microscopy. *Chem. Rev.* **2014**, *114*, 3120−3188.

(9) Rajendran, A.; Endo, M.; Sugiyama, H. State-of-the-art high-speed atomic force microscopy for investigation of single-molecular dynamics of proteins. *Chem. Rev.* **2014**, *114*, 1493−1520.

(10) Schwaderer, P.; Funk, E.; Achenbach, F.; Weis, J.; Bräuchle, C.; Michaelis, J. Single-molecule measurement of the strength of a siloxane bond. *Langmuir* **2008**, *24*, 1343−1349.

(11) Karthikeyan, S.; Potisek, S. L.; Piermattei, A.; Sijbesma, R. P. Highly efficient mechanochemical scission of silver-carbene coordination polymers. *J. Am. Chem. Soc.* **2008**, *130*, 14968−14969.

(12) Piermattei, A.; Karthikeyan, S.; Sijbesma, R. P. Activating catalysts with mechanical force. *Nat. Chem.* **2009**, *1*, 133−137.

(13) Li, Y.; Wen, J.; Qin, M.; Cao, Y.; Ma, H.; Wang, W. Single-molecule mechanics of catechol-iron coordination bonds. *ACS Biomater. Sci. Eng.* **2017**, *3*, 979−989.

(14) Wei, W.; Sun, Y.; Zhu, M.; Liu, X.; Sun, P.; Wang, F.; Gui, Q.; Meng, W.; Cao, Y.; Zhao, J. Structural insights and the surprisingly low mechanical stability of the Au-S bond in the gold-specific protein GolB. *J. Am. Chem. Soc.* **2015**, *137*, 15358−15361.

(15) Perales-Calvo, J.; Lezamiz, A.; Garcia-Manyes, S. The mechanochemistry of a structural zinc finger. *J. Phys. Chem. Lett.* **2015**, *6*, 3335−3340.

(16) Beedle, A. E.; Lezamiz, A.; Stirnemann, G.; Garcia-Manyes, S. The mechanochemistry of copper reports on the directionality of unfolding in model cupredoxin proteins. *Nat. Commun.* **2015**, *6*, 7894.

(17) Zheng, P.; Li, H. Highly covalent ferric-thiolate bonds exhibit surprisingly low mechanical stability. *J. Am. Chem. Soc.* **2011**, *133*, 6791−6798.

(18) Zheng, P.; Takayama, S.-I. J.; Mauk, A. G.; Li, H. Hydrogen bond strength modulates the mechanical strength of ferric-thiolate bonds in rubredoxin. *J. Am. Chem. Soc.* **2012**, *134*, 4124−4131.

(19) Zheng, P.; Chou, C.-C.; Guo, Y.; Wang, Y.; Li, H. Single molecule force spectroscopy reveals the molecular mechanical anisotropy of the FeS₄ metal center in rubredoxin. *J. Am. Chem. Soc.* **2013**, *135*, 17783−17792.

(20) Zheng, P.; Takayama, S.-I. J.; Mauk, A. G.; Li, H. Single molecule force spectroscopy reveals that iron is released from the active site of rubredoxin by a stochastic mechanism. *J. Am. Chem. Soc.* **2013**, *135*, 7992−8000.

(21) Zheng, P.; Wang, Y.; Li, H. Reversible unfolding-refolding of rubredoxin: a single-molecule force spectroscopy study. *Angew. Chem., Int. Ed.* **2014**, *53*, 14060−14063.

(22) Zheng, P.; Arantes, G. M.; Field, M. J.; Li, H. Force-induced chemical reactions on the metal centre in a single metalloprotein molecule. *Nat. Commun.* **2015**, *6*, 7569.

(23) Arantes, G. M.; Bhattacharjee, A.; Field, M. J. Homolytic cleavage of Fe-S bonds in rubredoxin under mechanical stress. *Angew. Chem., Int. Ed.* **2013**, *52*, 8144−8146.

(24) Arantes, G. M.; Field, M. J. Ferric-thiolate bond dissociation studied with electronic structure calculations. *J. Phys. Chem. A* **2015**, *119*, 10084−10090.

(25) Zheng, P.; Cao, Y.; Li, H. Facile method of constructing polyproteins for single-molecule force spectroscopy studies. *Langmuir* **2011**, *27*, 5713−5718.

(26) Li, Y. D.; Lamour, G.; Gsponer, J.; Zheng, P.; Li, H. The molecular mechanism underlying mechanical anisotropy of the protein GB1. *Biophys. J.* **2012**, *103*, 2361−2368.

(27) Grubmuller, H.; Heymann, B.; Tavan, P. Ligand binding: molecular mechanics calculation of the streptavidin-biotin rupture force. *Science* **1996**, *271*, 997−999.

(28) Izrailev, S.; Stepaniants, S.; Balsera, M.; Oono, Y.; Schulten, K. Molecular dynamics study of unbinding of the avidin-biotin complex. *Biophys. J.* **1997**, *72*, 1568−1581.

(29) Lim, B. B. C.; Lee, E. H.; Sotomayor, M.; Schulten, K. Molecular basis of fibrin clot elasticity. *Structure* **2008**, *16*, 449−459.

(30) Lu, H.; Isralewitz, B.; Krammer, A.; Vogel, V.; Schulten, K. Unfolding of titin immunoglobulin domains by steered molecular dynamics simulation. *Biophys. J.* **1998**, *75*, 662−671.

(31) Lee, E. H.; Hsin, J.; Sotomayor, M.; Comellas, G.; Schulten, K. Discovery through the computational microscope. *Structure* **2009**, *17*, 1295−1306.

(32) Liang, J.; Fernández, J. M. Mechanochemistry: one bond at a time. *ACS Nano* **2009**, *3*, 1628−1645.

(33) Ribas-Arino, J.; Marx, D. Covalent mechanochemistry: theoretical concepts and computational tools with applications to molecular nanomechanics. *Chem. Rev.* **2012**, *112*, 5412−5487.

(34) Groote, R.; Jakobs, R. T. M.; Sijbesma, R. P. Mechanocatalysis: forcing latent catalysts into action. *Polym. Chem.* **2013**, *4*, 4846−4859.

(35) Makarov, D. E. Perspective: mechanochemistry of biological and synthetic molecules. *J. Chem. Phys.* **2016**, *144*, 030901.

(36) Lupton, E. M.; Nonnenberg, C.; Frank, I.; Achenbach, F.; Weis, J.; Bräuchle, C. Stretching siloxanes: an ab initio molecular dynamics study. *Chem. Phys. Lett.* **2005**, *414*, 132−137.

(37) Barros, T. C.; Yunes, S.; Menegon, G.; Nome, F.; Chaimovich, H.; Politi, M. J.; Dias, L. G.; Cuccovia, I. M. Hydrolysis of 1,8-and 2,3-naphthalic anhydrides and the mechanism of cyclization of 1,8-

naphthalic acid in aqueous solutions. *J. Chem. Soc. Perkin Trans. 2* **2001**, *12*, 2342−2350.

(38) Groote, R.; Szyja, B. M.; Pidko, E. A.; Hensen, E. J. M.; Sijbesma, R. P. Unfolding and mechanochemical scission of supramolecular polymers containing a metal-ligand coordination bond. *Macromolecules* **2011**, *44*, 9187−9195.

(39) Kochhar, G. S.; Heverly-Coulson, G. S.; Mosey, N. J. In *Polymer Mechanochemistry*; Boulatov, R., Ed.; Springer International Publishing, 2015; pp 37−96.

(40) Stauch, T.; Dreuw, A. Advances in quantum mechanochemistry: electronic structure methods and force analysis. *Chem. Rev.* **2016**, *116*, 14137−14180.

(41) Senftle, T. P.; Hong, S.; Islam, M. M.; Kylasa, S. B.; Zheng, Y.; Shin, Y. K.; Junkermeier, C.; Engel-Herbert, R.; Janik, M. J.; Aktulga, H. M.; Verstraelen, T.; Grama, A.; van Duin, A. C. T. The ReaxFF reactive force-field: development, applications and future directions. *npj Comput. Mater.* **2016**, *2*, 15011.

(42) Bau, R.; Rees, D. C.; Kurtz, D. M.; Scott, R. A.; Huang, H.; Adams, M. W. W.; Eidsness, M. K. Crystal structure of rubredoxin from *Pyrococcus furiosus* at 0.95 Angstroms resolution, and the structures of N-terminal methionine and formylmethionine variants of Pf Rd. Contributions of N-terminal interactions to thermostability. *JBIC, J. Biol. Inorg. Chem.* **1998**, *3*, 484−493.

(43) *PyMOL*, The PyMOL Molecular Graphics System, version 1.2r2; Schrödinger, LLC: New York.

(44) MacKerell, A. D.; Bashford, D.; Bellott, M.; Dunbrack, R. L.; Evanseck, J. D.; Field, M. J.; Fischer, S.; Gao, J.; Guo, H.; Ha, S.; Joseph-McCarthy, D.; Kuchnir, L.; Kuczera, K.; Lau, F. T. K.; Mattos, C.; Michnick, S.; Ngo, T.; Nguyen, D. T.; Prodhom, B.; Reiher, W. E.; Roux, B.; Schlenkrich, M.; Smith, J. C.; Stote, R.; Straub, J.; Watanabe, M.; Wiórkiewicz-Kuczera, J.; Yin, D.; Karplus, M. All-atom empirical potential for molecular modeling and dynamics studies of proteins. *J. Phys. Chem. B* **1998**, *102*, 3586−3616.

(45) MacKerell, A. D.; Feig, M.; Brooks, C. L. Extending the treatment of backbone energetics in protein force fields: Limitations of gas−phase quantum mechanics in reproducing protein conformational distributions in molecular dynamics simulations. *J. Comput. Chem.* **2004**, *25*, 1400−1415.

(46) Chang, C. H.; Kim, K. Density functional theory calculation of bonding and charge parameters for molecular dynamics studies on [FeFe] hydrogenases. *J. Chem. Theory Comput.* **2009**, *5*, 1137−1145.

(47) Carvalho, A. T. P.; Teixeira, A. F. S.; Ramos, M. J. Parameters for molecular dynamics simulations of iron-sulfur proteins. *J. Comput. Chem.* **2013**, *34*, 1540−1548.

(48) Yelle, R. B.; Park, N.-S.; Ichiye, T. Molecular dynamics simulations of rubredoxin from Clostridium pasteurianum: changes in structure and electrostatic potential during redox reactions. *Proteins: Struct., Funct., Genet.* **1995**, *22*, 154−167.

(49) Still, W. C.; Tempczyk, A.; Hawley, R. C.; Hendrickson, T. Semianalytical treatment of solvation for molecular mechanics and dynamics. *J. Am. Chem. Soc.* **1990**, *112*, 6127−6129.

(50) Qiu, D.; Shenkin, P.; Hollinger, F.; Still, W. The GB/SA continuum model for solvation. A fast analytical method for the calculation of approximate Born radii. *J. Phys. Chem. A* **1997**, *101*, 3005−3014.

(51) Schaefer, M.; Bartels, C.; Karplus, M. Solution conformations and thermodynamics of structured peptides: molecular dynamics simulation with an implicit solvation model. *J. Mol. Biol.* **1998**, *284*, 835−848.

(52) Morse, P. M. Diatomic molecules according to the wave mechanics. II. Vibrational levels. *Phys. Rev.* **1929**, *34*, 57−64.

(53) Parr, R. G.; Yang, W. *Density-Functional Theory of Atoms and Molecules*, 1st ed.; Oxford University Press, 1996.

(54) Byrd, R. H.; Lu, P.; Nocedal, J.; Zhu, C. A limited memory algorithm for bound constrained optimization. *SIAM J. Scientif. Statistic. Comput.* **1995**, *16*, 1190−1208.

(55) Zhu, C.; Byrd, R. H.; Lu, P.; Nocedal, J. L-BFGS-B: Algorithm 778: L-BFGS-B, FORTRAN routines for large scale bound constrained optimization. *ACM Trans. Math. Softw.* **1997**, *23*, 550−560.

(56) Pronk, S.; Páll, S.; Schulz, R.; Larsson, P.; Bjelkmar, P.; Apostolov, R.; Shirts, M. R.; Smith, J. C.; Kasson, P. M.; van der Spoel, D.; Hess, B.; Lindahl, E. GROMACS 4.5: a high-throughput and highly parallel open source molecular simulation toolkit. *Bioinformatics* **2013**, *29*, 845−854.

(57) Hess, B.; Bekker, H.; Berendsen, H. J. C.; Fraaije, J. G. E. M. LINCS: A linear constraint solver for molecular simulations. *J. Comput. Chem.* **1997**, *18*, 1463−1472.

(58) Stirnemann, G.; Giganti, D.; Fernandez, J. M.; Berne, B. J. Elasticity, structure, and relaxation of extended proteins under force. *Proc. Natl. Acad. Sci. U. S. A.* **2013**, *110*, 3847−3852.

(59) Marko, J. F.; Siggia, E. D. Stretching DNA. *Macromolecules* **1995**, *28*, 8759−8770.

(60) Dietz, H.; Rief, M. Protein structure by mechanical triangulation. *Proc. Natl. Acad. Sci. U. S. A.* **2006**, *103*, 1244−1247.

(61) Hummer, G.; Szabo, A. Kinetics from nonequilibrium single-molecule pulling experiments. *Biophys. J.* **2003**, *85*, 5−15.

(62) Yu, H.; Siewny, M. G. W.; Edwards, D. T.; Sanders, A. W.; Perkins, T. T. Hidden dynamics in the unfolding of individual bacteriorhodopsin proteins. *Science* **2017**, *355*, 945−950.

(63) Bell, G. Models for the specific adhesion of cells to cells. *Science* **1978**, *200*, 618−627.

(64) Evans, E.; Ritchie, K. Dynamic strength of molecular adhesion bonds. *Biophys. J.* **1997**, *72*, 1541−1555.

(65) Rief, M.; Fernandez, J. M.; Gaub, H. E. Elastically coupled two-level systems as a model for biopolymer extensibility. *Phys. Rev. Lett.* **1998**, *81*, 4764−4767.

(66) Dudko, O. K.; Hummer, G.; Szabo, A. Intrinsic rates and activation free energies from single-molecule pulling experiments. *Phys. Rev. Lett.* **2006**, *96*, 108101.

(67) Ainavarapu, S. R. K.; Brujić, J.; Huang, H. H.; Wiita, A. P.; Lu, H.; Li, L.; Walther, K. A.; Carrion-Vazquez, M.; Li, H.; Fernandez, J. M. Contour length and refolding rate of a small protein controlled by engineered disulfide bonds. *Biophys. J.* **2007**, *92*, 225−233.

(68) Cavagnero, S.; Zhou, Z. H.; Adams, M. W. W.; Chan, S. I. Unfolding mechanism of rubredoxin from *Pyrococcus furiosus*. *Biochemistry* **1998**, *37*, 3377−3385.

(69) Cavagnero, S.; Zhou, Z. H.; Adams, M. W. W.; Chan, S. I. Response of rubredoxin from *Pyrococcus furiosus* to environmental changes: implications for the origin of hyperthermostability. *Biochemistry* **1995**, *34*, 9865−9873.